Supplementary material for Point defects on graphene on metals

M. M. Ugeda,[1] D. Fernández-Torre,[2] I. Brihuega,[1,*] P. Pou,[2] A. J. Martínez-Galera,[1] R. Pérez,[2] and J. M. Gómez-Rodríguez[1]

[1] *Departamento de Física de la Materia Condensada, Universidad Autónoma de Madrid, E-28049 Madrid, Spain*

[2] *Departamento de Física Teórica de la Materia Condensada, Universidad Autónoma de Madrid, E-28049 Madrid, Spain*

OBSERVATION OF INTERVALLEY SCATTERING PROCESSES IN GRAPHENE ADSORBED ON PT(111)

In ideal graphene, atomic size impurities give rise to intervalley scattering processes [1] which are reflected into short wavelength modulations of the LDOS with $(\sqrt{3}\times\sqrt{3})R30^o$periodicity (R3 in the following). In well decoupled graphene layers, as epitaxial graphene on SiC or HOPG surfaces, such R3 patterns associated with the presence of point defects have been observed by means of low bias STM images, which are a measure of the LDOS at E_F [2–6]. In addition, 2D Fourier transforms (FT) of conductance images measured at different energies on graphene on SiC, have allowed to measure graphene's linear energy dispersion [4] or to assess its electronic quirality [5].

Here, despite being in a decoupled graphene on metal system, the extension of the perturbation generated by atomic vacancies is much shorter than in the SiC or HOPG cases. Therefore, in order to have enough signal as to be able to obtain some valuable information, it was necessary introduce a higher density of vacancies by exposing the sample to higher doses of Ar^+ ions. Fig S1a shows one region of a heavily sputtered sample presenting a high density of generated C vacancies, where the presence of R3 scattering patterns between defects can be clearly observed. As stated before, such R3 patterns correspond to intervalley scattering processes as the one illustrated in Fig S1b. In graphene, the Brillouin zone presents six circular pockets around K symmetry points, whose radius k depends on the energy distance with respect to the Dirac point. In the graphene/Pt(111) case, our LDOS spectra shows that E_D is located ∼300mV above Fermi energy, so, assuming a Fermi velocity 10^6 m/s as recently measured by photoemission [7], one can estimate the expected radius k of such pockets as a function of energy (see S1b). Fig S1c, corresponds to a 2D FT of a conductance image measured at -50mV on the same region than FigS1a, but on a larger area ($80\times80nm^2$). Six red points are observed in the low frequency zone of the FT, which correspond to the $2\sqrt{21}\times\sqrt{21}$ R(11°) moiré periodicity. In addition, circular features due to intervalley scattering processes can be identified in the R3 zones (see also fig S1e). By measuring the radial average of such circular features, we can obtain a measure of the k vector for the corresponding energy. In the present case, we obtain k(-50meV)=$0.5\pm0.1nm^{-1}$ in good agreement with our expectations. Although the short extension of the R3 perturbation generated here by point defects does not provide enough signal to our FT as to extract a clear energy dispersion of the graphene adsorbed on Pt(111) system, or to try to investigate its electronic quirality, our results are a further confirmation of an scenario where the graphene adsorbed on Pt(111) is hole doped with E_D located 300 meV above the Fermi energy and presenting the same Fermi velocity of 10^6 m/s as free standing graphene.

THEORETICAL METHOD

We have calculated all structural and electronic properties (band structures and DOS) using DFT as implemented in the VASP code [8]. For these calculations we employed the PBE functional [9] empirically corrected to include van der Waals interactions [10], projector augmented wave (PAW) pseudopotentials [11], and a plane-wave cutoff of 400 eV. We constructed two kinds of supercells, one to represent the 3×3 graphene/Pt(111) moiré system, and another to represent the C vacancy in graphene/Pt(111). The first consisted of a single sheet of graphene and 4 layers of Pt, and the second was a 2×2 reproduction of the previous with a single C atom removed, and a total of 183 atoms. The mismatch between C and Pt lattices in the 3×3 moiré of graphene/Pt(111) is small (0.6 %), and in our calculations we decided to fix the size of the supercell to match the relaxed graphene lattice (a_0 = 2.46 Å). For the structural relaxations, we fixed the positions of the atoms in the two lowest Pt layers, leaving the other atoms free to relax. The final structures correspond to energies converged better than 10^{-6} eV/atom and forces smaller than 0.04 eV/Å. As the graphene sheet was allowed to move freely during the relaxations, in the vacancy system its final position is displaced with respect to the relaxed moiré. For the DOS and band structure calculations, we first evaluated the

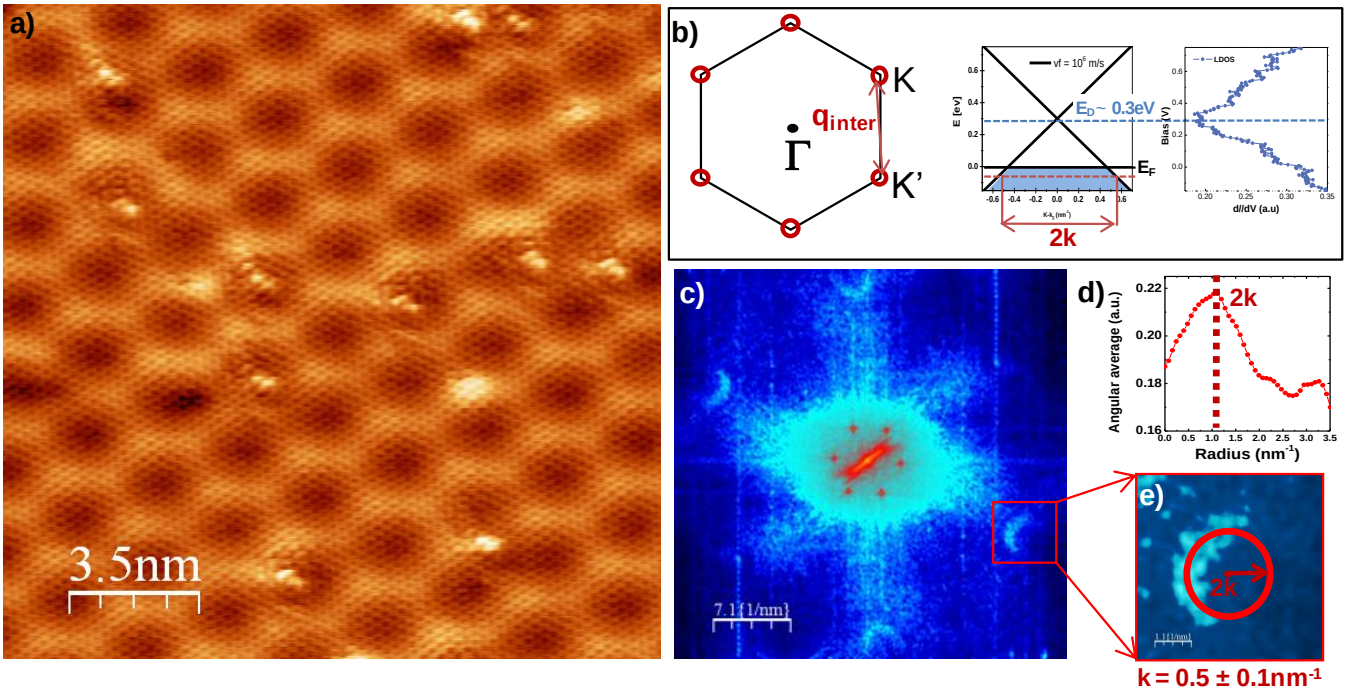

FIG. 1: a) 17.5×17.5nm^2 STM image of a region with a high density of vacancies. Sample voltage: -8mV. b) Left, schematic representation of the graphene 2D Brillouin zone with red circles as constant energy contours and the red arrow illustrating an intervalley scattering process. Middle, schematic band structure of hole doped graphene with E_D =+300meV and v_F =106m/s. Right, experimental dI/dV spectra showing a V shaped dip at +300mV indicating E_D position. c) 2D FT of a conductance image measured at -50mV in a zoom out of panel a). d) Angular average of the circular feature around the K points outlined in panel c). e) Zoom in showing the circular feature around K outlined in c). A red circle of radius 2k is drawn.

electronic charge over a 3×3 Γ-centered Monkhorst-Pack grid, and then calculated the bands and DOS over a 51×51 Γ-centered Monkhorst-Pack grid for the moiré system, and over an equivalent 25×25 k-mesh for the vacancy system.

The calculation of the STM currents is based on nonequilibrium Keldysh-Green function techniques, the details of the implementation are presented in Ref. [12]. We have used an idealized Pt tip with just one atom and a single dz^2 orbital. We have found that this idealized apex enhances the atomic contrast of the theoretical STM images making them easier to interpret. The STM method requires the mapping of the Hamiltonian in a local orbital basis. In this work, we have used the OpenMX code [13–15] with a single-zeta basis set and the PBE approach for the exchange-correlation interaction. We have used the atomic structure obtained by the PBE+vdw method implemented in VASP. We have tested that the electronic properties (in particular the Projected DOS) calculated with both methods are very similar. The STM images are calculated with a mesh of 2050 (441) k-points to sample the 2D Brillouin zone of the 3×3 (6×6) surface cell. Due to the size of the cell and the high number of k points required to converge the calculation, multiple scattering effects are not included in the current calculation. We have confirmed that, in this system, this simplification provides a very good approach and drastically reduces the required computational resources.

QUENCHING OF THE MAGNETISM ASSOCIATED TO THE VACANCY ON GRAPHENE/PT(111)

The best way to understand the disappearance of the magnetic moment in the Graphene/Pt(111) system is the comparison with the case of a single vacancy on graphene. The quenching of the magnetic moment results from the interplay of two main effects: (1) the doping of the graphene layer induced by the metal, and (2) the broadening of the defect levels and the distortion of the vacancy structure associated with the graphene-substrate interaction.

The calculated ground state (GS) of a single vacancy on graphene is magnetic [16, 17]. The geometry of the atoms in this GS is nearly planar, and the associated magnetic moment of $\sim 1.5\mu_B$ results from two contributions: (i) a σ state, essentially of sp^2 character and strongly localized on the single unpaired C atom surrounding the vacancy, that contributes $\sim 1\mu_B$; and (ii) a π state, associated with the p_z states that are normal to the graphene plane

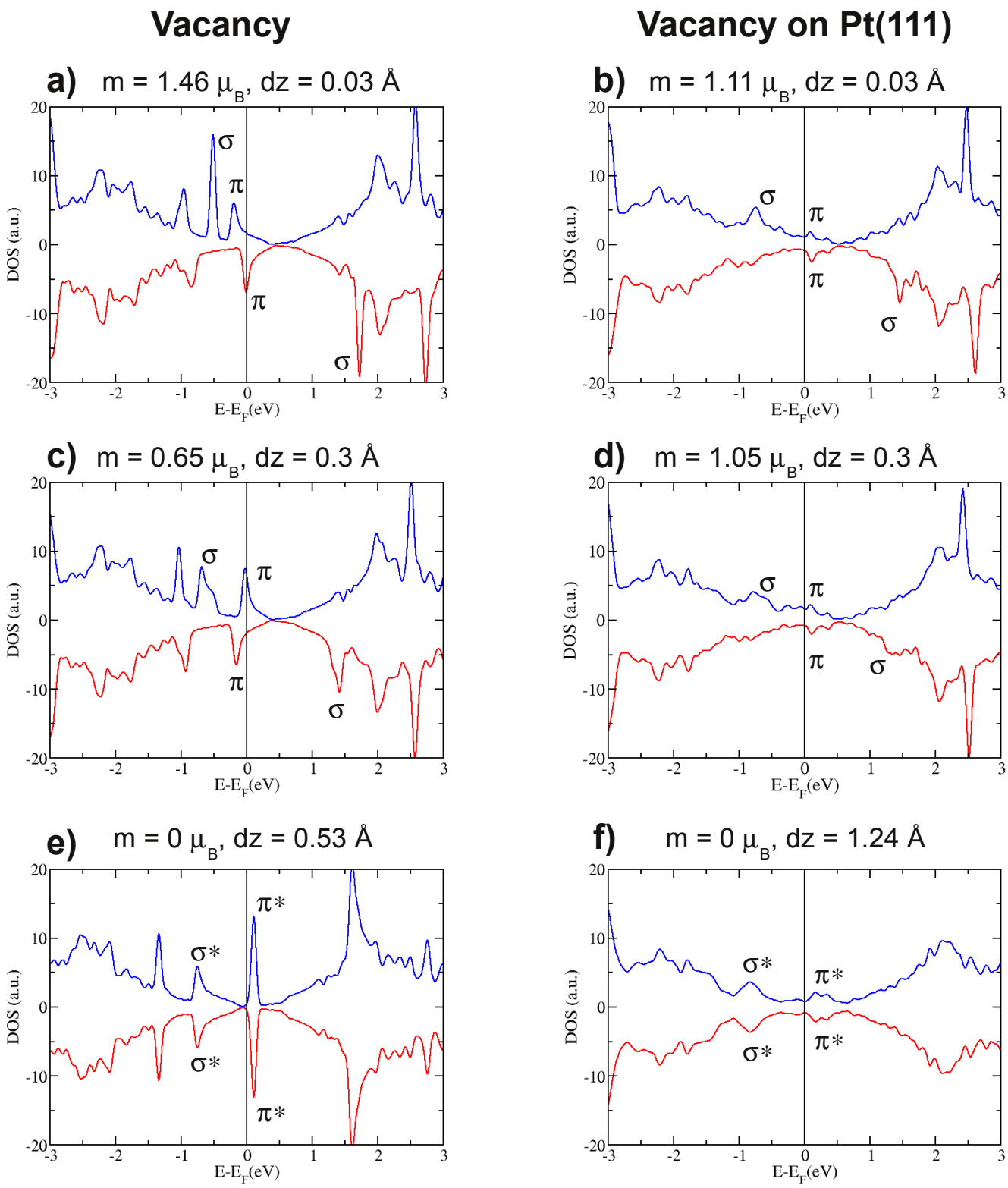

FIG. 2: Projection of the DOS on the C atoms for different atomic configurations of a single vacancy on graphene (a), c), and e)), and for the same system on top of a Pt(111) slab (b), d), and f)). In each panel, we indicate the magnetic moment (m), the displacement of the single unpaired C atom with respect to the C sheet (dz), and the character (σ,π) of the peaks near the Fermi level. In the non-magnetic solutions, the labels $\sigma*$ and $\pi*$ recalled the former symmetry of those peaks that have now a mixed character. The DOS in a) and f) correspond to the GS for the vacancy and the vacancy on Pt(111), respectively.

and delocalized over the atoms of the sublattice opposite to the vacancy, with major contributions coming from the atoms that are closest. These are the two states that are highlighted in the majority spin DOS (blue line) shown in Fig. 2a. The magnetic contribution of the majority-spin π state is partially compensated by the contribution of the minority-spin π state (red line) close to the Fermi level, resulting in a total π contribution of $\sim 0.5\mu_B$.

The single vacancy on graphene has a non-magnetic state that is only +0.1 eV above the GS. In this case, the associated geometry is non-planar, with the single unpaired C atom moving about 0.5 Å out of the graphene plane. The key to understand the absence of a magnetic moment can be found in the spin-DOS shown for an intermediate state where the atom has displaced just 0.3 Å out of plane (Fig. 2c). The outward displacement mixes the σ and π states and, thus, changes the hybridization of that atom. This effect induces the broadening of the former σ state and pushes the π state of the same spin to the fermi level, changing the relative occupation of the two π states and reducing the magnetic moment. In the final relaxed structure (Fig. 2e), both states are completely mixed in a bonding and antibonding combinations, and the stable electronic configuration corresponds to a double occupancy of the bonding σ^* state.

The analysis described above suggest to attack the problem of the absence of magnetism in the Graphene/Pt system in two steps: Firstly, we take the GS structure of the vacancy on graphene, locate it on top of the Pt at the final graphene-Pt distance and calculate the electronic properties and the magnetic moment for that configuration. Then, we let the system to relax towards the minimum energy configuration and check the evolution of the magnetic moment. The results of the first step are shown in Figure 2b. The interaction with the Pt broadens the sharp levels found in the graphene case. However, this configuration is still magnetic, but with a reduced magnetic moment compared with the graphene case. This reduction is associated with the doping effect due to Fermi level alignment between the graphene and the Pt surface. The C π states of both spins are shifted above the Fermi level, and its contribution to the magnetic moment is lost (see Fig 2.b).

The evolution of the system as it relaxes towards the ground state configuration is illustrated in Figures 2d and 2f. During the relaxation, the single unpaired C atom moves out of the plane and towards the Pt by more than 1 Å reducing the magnetic moment (Fig. 2d) and ending up in a non-magnetic state (Fig. 2e). Comparing the DOS of the two equivalent geometries in the isolated graphene and the graphene/Pt cases, we find a similar electronic structure but with the former σ and π peaks (now they have a mixed character) significantly broadened by the interaction with the Pt. The driving force for this relaxation is the interaction between the dangling bond of the single unpaired atom and the d states of the Pt surface: The energy gain by such a new bond formation is much larger than the energy difference between the magnetic and non-magnetic states of the single vacancy on graphene.

In summary, the reactive character of the vacancy on graphene is ultimately responsible for the lost of magnetism upon interaction with a Pt substrate. We believe the same effect will be present when graphene is deposited on other transition metal surfaces, and in the case of other magnetic (and reactive) defects on graphene, such as double vacancies or edges.

THEORETICAL RESULTS: DOS RESONANCE ABOVE THE FERMI LEVEL

As discussed in the Letter, our STS measurements show a broad resonance in the LDOS above the Fermi level associated with vacancies in graphene/Pt(111). In order to illustrate the link between this peak and the presence of a vacancy, we also compare the isolated graphene and the graphene/Pt cases. Figure 3 shows the calculated density of states projected on the C atoms for the two non-magnetic solutions described in the previous section. The sum of the LDOS over all C atoms has a single peak above E_F centered at +0.1 eV for the vacancy on graphene (Fig 3.a), and a more structured feature centered at about +0.25 eV for the vacancy on graphene/Pt(111) (Fig 3.b). The shift between the centers of these two resonances can be assigned to doping effects, as discussed in the previous section. The fact that the feature at +0.25 eV is much broader can be also associated with the coupling to the Pt substrate.

In order to illustrate the origin of this peak, we include three additional curves in Figure 3: the projection of the LDOS on the C atoms belonging to the two different graphene sublattices, the one containing the defect (labelled B in Fig. 3), and its complementary (sublattice A); and the sum of the LDOS on the 6 nearest neighbors to the vacancy belonging to sublattice A. As can be seen in Figure 3, these 6 atoms are responsible for about half of the intensity of the peak, but, in order to recover most of the intensity, all of the atoms in sublattice A need to be taken into account. From the projections of the LDOS on the atomic orbitals of these C atoms (not shown), we conclude that most of the peak comes from p_z orbitals. Therefore, the observed STS resonance above the Fermi level can be assigned to a π band delocalized over the atoms of sublattice A, with the largest contributions coming from the atoms closest to the vacancy.

The experimental peak is reproduced only qualitatively by the theoretical calculations, as its center was at about

+0.5 eV and its FWHM was of only 0.15 eV. We think that this discrepancy is due to the small size of our unit cell. Even a relatively large 6x6 unit cell is not enough to model accurately some of the properties of an isolated vacancy. The periodically repeated vacancies interact quite strongly both elastically (through the strain created on the graphene layer) and electronically (mediated in part by the Pt substrate). This interaction affects the detailed position and width of the empty states giving rise to the observed resonance. Although calculations with larger unit cells are feasible in the case of a pure graphene layer, they are beyond the capabilities of the plane-wave implementation of DFT that we have used due to the heavy computational burden imposed by the Pt slab. Furthermore, even simulations with very large unit cells for a graphene sheet fail to reproduce the correct position of the Fermi level, for a single, isolated vacancy [16]: it still appears 0.2 eV below the Dirac point for the largest systems considered.

However, we have to emphasize that calculations with the 6x6 unit cell are enough to support our main conclusions. Regarding the magnetic properties, previous studies of the system-size dependence for single graphene sheets with vacancies [16] conclude that the magnetic moment was already converged for a number of C atoms similar to the one considered in our calculations. Furthermore, the mechanism revealed for the quenching of the magnetism, the out-of-plane relaxation of the unpaired carbon atom close to the vacancy, is very local.

Our calculations also provide a good description of the spatial extent close to the vacancy of the states giving rise to the resonance, as shown by the agreement between the simulated STM images and the experiment. We have already pointed out in the manuscript our possible limitation in the theoretical description of the decay of these states far from the vacancy due to finite-size effects. These spurious interactions between the tails of the π states do not modify significantly the spatial distribution of the associated wavefunction close to vacancy but are crucial to determine the energy position and width of the resonance.

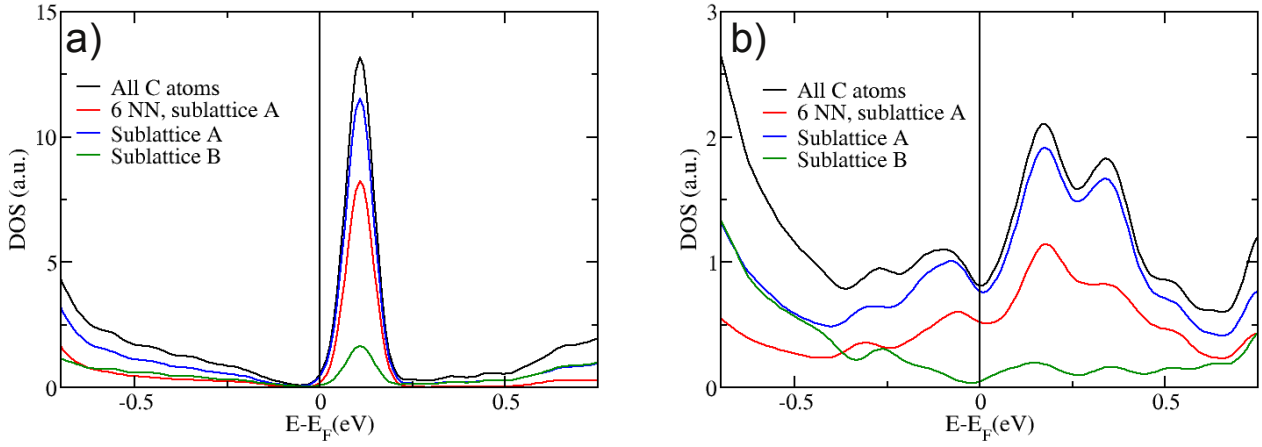

FIG. 3: DOS projected on the C atoms for (a) a single C vacancy on graphene (non-magnetic solution) and (b) a single C vacancy on graphene over Pt(111) (GS solution, also non-magnetic). The projected DOS are summed over: (1) all the C atoms (black lines), (2) the 6 nearest-neigbours to the vacancy belonging to sublattice A (red lines, see text), (3) all C atoms in sublattice A (blue lines), and (4) all C atoms in sublattice B (green lines, see text). We should note that, in all the cases, the LDOS has essentially a p-character in the displayed energy range

* Corresponding author.
Email address: ivan.brihuega@uam.es

[1] T. Ando, T. Nakanishi, and R. Saito, J. Phys. Soc. Jpn. **67**, 2857 (1998).
[2] K. F. Kelly, D. Sarkar, G. D. Hale, S. J. Oldenburg, and N. J. Halas, Science **273**, 1371 (1996).
[3] P. Mallet, F. Varchon, C. Naud, L. Magaud, C. Berger, and J. Y. Veuillen, Phys. Rev. B **76** (2007).
[4] G. M. Rutter, J. N. Crain, N. P. Guisinger, T. Li, P. N. First, and J. A. Stroscio, Science **317**, 219 (2007).
[5] I. Brihuega, P. Mallet, C. Bena, S. Bose, C. Michaelis, L. Vitali, F. Varchon, L. Magaud, K. Kern, and J. Y. Veuillen, Phys. Rev. Lett. **101** (2008).
[6] M. M. Ugeda, I. Brihuega, F. Guinea, and J. M. Gomez-Rodriguez, Phys. Rev. Lett. **104** (2010).
[7] P. Sutter, J. T. Sadowski, and E. Sutter, Phys. Rev. B **80** (2009).
[8] G. Kresse and J. Furthmüller, Phys. Rev. B **54**, 11169 (1996).
[9] J. P. Perdew, K. Burke, and M. Ernzerhof, Phys. Rev. Lett. **77**, 3865 (1996).

[10] S. Grimme, J. Comp. Chem. **27**, 1787 (2006).
[11] G. Kresse and D. Joubert, Phys. Rev. B **59**, 1758 (1999).
[12] J. M. Blanco, F. Flores, and R. Perez, Prog. Surf. Sci. **81**, 403 (2006).
[13] The code, OPENMX, pseudoatomic basis functions, and pseudopotentials are available on the website: http://www.openmx-square.org/.
[14] T. Ozaki, Phys. Rev. B **67**, 155108 (2003).
[15] T. Ozaki, H. Kino, Phys. Rev. B **72**, 045121 (2005).
[16] O. V. Yazyev and L. Helm, Phys. Rev. B **75**, 125408 (2007).
[17] Y. Ma, P. O. Lehtinen, A. S. Foster, and R. M. Nieminen, New. J. Phys. **6**, 68 (2004).